Astronomy & Astrophysics manuscript no. Andreanietal-APEXSEPIA5
November 10, 2018

Extreme conditions in the molecular gas of lensed star-forming galaxies at z∼3

Paola Andreani[1], Edwin Retana-Montenegro[2], Zhi-Yu Zhang[1, 3], Padelis Papadopoulos[4, 5, 6], Chentao Yang[7], and Simona Vegetti[8]

[1] European Southern Observatory, Karl-Schwarzschild-Straße 2, 85748 Garching, Germany e-mail: `pandrean@eso.org`
[2] Leiden Observatory, Leiden University, P.O. Box 9513, 2300 RA, Leiden,The Netherlands e-mail: `eretana@strw.leidenuniv.nl`
[3] Institute of Astronomy, University of Edinburgh, Royal Observatory, Blackford Hill, Edimburgh EH9 3HJ, UK
[4] Department of Physics, Section of Astrophysics, Astronomy and Mechanics, Aristotle University of Thessaloniki, Thessaloniki, Macedonia, 54124, Greece
[5] Research Center for Astronomy, Academy of Athens, Soranou Efesiou 4, GR-115 27 Athens, Greece
[6] School of Physics and Astronomy, Cardiff University, Queen's Buildings, The Parade, Cardiff, CF24 3AA, UK
[7] European Southern Observatory, Alonso de Cordova, 3107, Vitacura, Casilla 19001, Santiago de Chile, Chile
[8] Max-Planck Institut für Astrophysik, Boltzmann strasse , 85748 Garching, Germany

Received ; accepted

ABSTRACT

Aims. Atomic Carbon can be an efficient tracer of the molecular gas mass, and when combined to the detection of high-J and low-J CO lines it yields also a sensitive probe of the power sources in the molecular gas of high redshift galaxies.

Methods. The recently installed SEPIA 5 receiver at the focus of the APEX telescope has opened up a new window at frequencies 159 - 211 GHz allowing the exploration of the Atomic Carbon in high-z galaxies, at previously inaccessible frequencies from the ground. We have targeted three gravitationally lensed galaxies at redshift of about 3 and conducted a comparative study of the observed high-J CO/CI ratios with well-studied nearby galaxies.

Results. Atomic Carbon (CI(2-1)) was detected in one of the three targets and marginally in a second, while in all three targets the $J = 7 \rightarrow 6$ CO line is detected.

Conclusions. The CO(7-6)/CI(2-1), CO(7-6)/CO(1-0) line ratios and the CO(7-6)/(far-IR continuum) luminosity ratio are compared to those of nearby objects. A large excitation status in the ISM of these high-z objects is seen, unless differential lensing unevenly boosts the CO line fluxes from the warm and dense gas more than the CO(1-0), CI(2-1), tracing a more widely distributed cold gas phase. We provide estimates of total molecular gas masses derived from the atomic Carbon and the Carbon monoxide CO(1-0), which within the uncertainties turn out to be equal.

Key words. galaxies: starburst – galaxies: ISM – ISM: molecules – ISM: abundances – submillimeter: galaxies – techniques: spectroscopic

1. Introduction

The initial conditions of star formation inside molecular clouds are set by the gas temperature, density, dynamical state and the local radiation field, as they determine the free fall time and the Jeans mass. Understanding these conditions is essential to fully understand the physics that drives the bulk of the star formation (SF), especially during the early phase in the Universe.

Atomic carbon (CI) forbidden fine-structure lines [1] have been proven to be a good or even a better tracer of the total molecular gas (H_2) compared to the traditional studies employing rotational transitions of carbon monoxide (CO) under a large range of physical conditions (Gerin & Phillips 2000; Papadopoulos et al. 2004; Tomassetti et al. 2014). They have emergent flux densities per H_2 column density higher than those of the low-CO rotational lines even at low metallicity and they are fully concomitant with CO line emission (Gerin & Phillips 2000; Papadopoulos et al. 2004; Alaghband-Zadeh et al. 2013).

The positive K-correction of the two CI lines versus the low-J CO transitions yet their similar excitation characteristics starts giving an advantage to the former at $z \gtrsim 0.5$. CI lines can remain well-excited for cooler, lower density molecular gas. This allows the use of CI lines as tracers of the molecular gas mass and gas-rich galaxy dynamics over a much larger fraction of cosmic look-back time. Finally, they are optically thin (i.e. no need for an X_{CO}-like factor), with only the $[C/H_2]$ abundance as their main source of uncertainty (an uncertainty common to all species that are not H_2 for e.g. ^{13}CO lines, or dust emission as H_2 gas mass estimators).

The two high-J CO lines with frequencies similar to the CI lines (J=4-3, 7-6), are typically bright in star forming (SF) galaxies, but trace only the dense and warm H_2 gas near star-forming regions, while the low-J CO and CI lines remain bright in relatively diffuse (10^3 cm^{-3}) and colder (∼ 10-30 k) gas phases. Furthermore, it is known that C is not limited only in

---

[1] The CI excited fine levels $^3P_1$ and $^3P_2$ lie 23.6 and 62.4 K above the ground state ($^3P_0$) and are therefore easily populated by particle collisions in the cold interstellar medium (ISM). Two magnetic-dipole transitions are allowed between the fine-structure levels: $^3P_1 \rightarrow {}^3P_0$ (CI(1-0)) has a rest frequency of 492.1607 GHz, while $^3P_2 \rightarrow {}^3P_1$ (CI(2-1)) of 809.3435 GHz.

a thin C→ CO transition zones of FUV-illuminated clouds (as predicted by Photon Dissociation Region (PDR) models) but remains concomitant with the entire CO-rich cloud and its distribution may actually even go beyond the CO-rich parts (e.g. Papadopoulos et al. 2004; Bisbas et al. 2015). Thus CO(high-J)/CI line luminosity ratios can be considered as good proxies of (warm, dense, SF gas)/(total H_2 gas) mass fraction, even as degeneracies between temperature, density, and line optical depths prevent us from attributing actual mass fractions to these line ratios.

Finally, although the emission of singly ionised Carbon fine structure transition, CII, is much brighter than CI, and has already been detected in high-z galaxies (z∼5-7 i.e. De Breuck et al. 2014; Knudsen et al. 2016; Hayatsu et al. 2017; Bradac et al. 2017), its emission traces ionised gas (HII) and atomic gas (HI) dominated regions, making the interpretation as H_2 gas mass distribution tracer cumbersome.

At very high redshifts CI lines are also much less affected by the Cosmic Microwave Background than the low-J CO lines (Zhang et al. 2016). Moreover, the CI abundance is less sensitive to the astrochemical effects of enhanced cosmic ray (CR) densities expected in starbursts (e.g., submillimetre galaxies (SMGs)) (Bisbas et al. 2015). CRs can effectively destroy CO throughout H_2 clouds, leaving C (but not much CII), and unlike FUV photons that only act on the surface of the H_2 clouds and produce CII, CRs destroy CO volumetrically and can make the clouds CO-invisible (Bisbas et al. 2017).

At redshifts z∼2-4, the CI lines are redshifted into observable windows from the ground. Several galaxies have been observed (Weiss et al. 2005; Pety et al. 2004; Walter et al. 2011; Alaghband-Zadeh et al. 2013; Omont et al. 2013; Yang et al. 2017; Bothwell et al. 2017; Popping et al. 2017,and references therein), showing that the SMGs share properties with local ultraluminous infrared galaxies and with less compact, local starburst galaxies, providing new evidence that many SMGs have extended SF distributions. The total molecular mass inferred from those CI observations was found to be in disagreement with that obtained via the traditional conversion factor between CO mass and H_2 (e.g. Popping et al. 2017).

Here we report the observations of CI(2-1) and the CO(7-6) lines towards three z ∼3 lensed SMGs redshifted into the side bands of the ALMA Band 5 receiver which has been installed at the APEX telescope and offered to the science community since 2015. These targets have been selected from the HATLAS catalogue of bright submillimetre lensed objects (Bussmann et al. 2013) because of their brightness and their spectroscopic redshift which allows the observations of the CI(2-1) within the SEPIA 5 receiver bandwidth.

2. The SEPIA 5/APEX observations

The observations have been carried out with the SEPIA Band 5 receiver (Belitsky et al. 2017) at the Atacama Pathfinder EXperiment (APEX, Güsten et al. 2006). The receiver covers the frequency range 159 - 211 GHz. The lower and upper sideband (LSB and USB) are separated by 12 GHz and each sideband is recorded by 2 XFFTS (eXtended bandwidth Fast Fourier Transform Spectrometer) units of 2.5 GHz each, with a 1GHz overlap.

The spectra have been smoothed to a spectral resolution of 20 kms^{-1} and the beam size is 35″. We use a Jy/K factor of 34 to convert between antenna temperature T_A^* and flux density assuming point sources [2] (Billade et al. 2012; Immer et al. 2016).

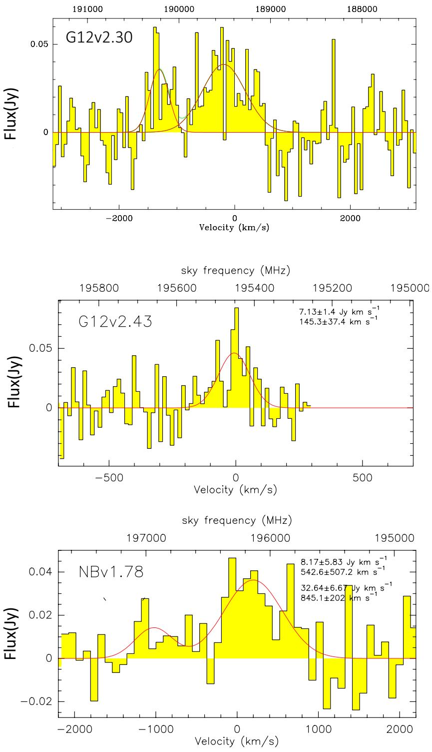

Fig. 1. Spatially integrated APEX/SEPIA5 spectra of the three lensed sources target of this work. The red lines represent the Gaussian fitting to the emission lines (CO(7-6) at ∼ zero velocities and CI(2-1)). Zero velocity are set to the CO(1-0) and CO(3-2) line sky frequency according to the previously measured spectroscopy redshifts given in Table 1

We conducted observations towards G12v2.43 during science verification (Project ID: 095.F-9803; PI: Andreani) and then for all the three sources during normal PI observing time using the wobbler switch mode with a precipitable water vapour (pwv) between 0.4 and 1.8mm. The observations were carried out for a total time of 9.6 hours, with 1, 2, 1.5 hours on source, respectively. Pointings were regularly checked on RW-LMi and IRC+10216 and a calibration scan was taken every 10 min. Data were reduced using CLASS/Gildas2. The SEPIA receiver was tuned at 189.3906, 195.42896 and 196.2085 GHz in the LSB, respectively. This corresponds to the redshifted frequencies between the two restframe frequencies 809.3 and 806.65 GHz of the CI(2-1) and CO(7-6) lines.

We removed a linear baseline from each individual spectrum before averaging the data. The rms reached are 1.0, 0.33, 0.7 mK respectively, at a 50 km s^{-1} resolution.

3. Results

3.1. Line ratio diagnostics

The spectra extracted from the SEPIA5 receiver are shown in Figure 1. The CO(7-6) line is clearly detected in all three sources

---

[2] http://www.eso.org/sci/activities/apexsv/sepia/sepia-band-5.html

Table 1. Observed line fluxes, velocities and luminosities

Galaxy	redshift	CO(7-6) $(Jy\ km/s)$	Δv (km/s)	CI(2-1) $(Jy\ km/s)$	Δv (km/s)	CO(1-0)^{a,b} $(Jy\ km/s)$	$\Delta v^{a,b}$ (km/s)	$L_{\rm FIR}{}^{c}$ ($10^{12} L_{\odot}$)	μ^{c}
J114637.9-001132 (G12v2.30)	3.2588	36.1±5.3	833±295	14.8±3.6	300±100	0.99±0.16	680±80	14.2±1.2	9.5 ± 0.6
J113526.3-014605 (G12v2.43)	3.1276	7.1±1.4	145±37	<6	<300	0.35±0.08	210±30	7.5±4.8	17 ± 11
J133800.8+245900 (NBv1.78)	3.1112	32.6±6.6	845±202	8.2±5.8	542±507	3.30± 0.50	560±70	12.3±1.4	13 ± 7

Notes.
[a] CO(1-0) data from Harris et al. (2012) [b] for NBv1.78 data are relative to the CO(3-2) transition, from Omont et al. (2013) [c] de-magnified values and magnification values from Zhang et al. (2018)

and the corresponding fluxes and line widths resulting from the Gaussian best fit are listed in Table 1.

The CI(2-1) line is detected at a 4σ level in G12v2.30, marginally ($\sim 2\sigma$) in NBv1.78 and not detected in G12v2.43. The corresponding fluxes or upper limits and line widths are listed in Table 1, together with the CO(1-0) fluxes taken from Harris et al. (2012), CO(3-2) in NBv1.78flux from Omont et al. (2013), the IR luminosities and magnification values from Zhang et al. (2018).

We use the line luminosity ratios $\frac{L'(CO(7-6))}{L'(CO(1-0))}$ and $\frac{L'(CO(7-6))}{L'(CI(2-1))}$ as proxies for the ratio between the warm (with T$\sim 100-150$K), dense (n$>\ 10^{4} cm^{-3}$) gas mass, $M_{\rm WD}$, and the total H_2 gas, $M_{\rm tot}(H_2)$, $M_{\rm WD}/M_{\rm tot}(H_2)$ mass fractions. Because the line radiative transfer model degeneracies prevent the computation of actual mass fractions, we use other galaxy-averaged ratios to place the gas conditions in the submm galaxies in perspective, and even examine whether the observed line ratios are compatible with only FUV-photon-driven energy sources for their ISM. This is important since PDRs have often been found inadequate to account for the global CO line excitation measured in many starbursts (Papadopoulos et al. 2012,and references therein). In placing our observed line ratios among the same ones measured for other galaxies where much more molecular and atomic line data allow a determination of their $M_{\rm WD}/M_{\rm tot}(H_2)$ mass fractions (and whether these are sustainable by FUV radiation fields), we can circumvent to some degree the aforementioned radiative transfer modelling uncertainties (which we do not attempt here), and examine the type of prevailing ISM power source in our galaxies as well.

In Figure 2 we compare the ratio $\frac{CO(7-6)}{CO(1-0)}$ between the line luminosities in K km s^{-1}pc^{2} for the sources listed in Table 1 with the same values for nearby galaxies (Kamenetzky et al. 2014; Rosenberg et al. 2015; Lu et al. 2017; Kamenetzky et al. 2017). For the extended objects we consider those whose fluxes are aperture-corrected (Kamenetzky et al. 2014). The CO line luminosity has been computed following Solomon et al. (1997).

We add in Figure 2 the corresponding values of the Milky Way taken from the COBE observations for the Galactic Centre (GC) (Fixsen et al. 1999). The corresponding values of similar lensed sources taken from the literature (Oteo et al. 2017; Yang et al. 2017; Walter et al. 2011), are also shown for comparison.

The histogram in Figure 2 can be used to examine the dominant power input of molecular gas reservoirs, whether it is provided by FUV-photons or dominated by some other mechanisms (e.g. CRs and/or turbulence).

In Figure 2 we add a dashed black vertical line splitting the values of the $\frac{CO(7-6)}{CO(1-0)}$ ratio between galaxies where other evidence demonstrated photon-heated molecular gas (low values), and objects with large ratios like the GC, the NGC253 nucleus and NGC 6240, systems where extensive studies of well sampled molecular SLEDs concluded non-FUV-photon driven power sources for their molecular gas reservoirs.

We detect a slight trend with the IR luminosity, i.e. lower $\frac{CO(7-6)}{CO(1-0)}$ are associated to galaxies with lower L(IR): values between 7 and 20 for luminous infrared galaxies (LIRGs) with L(IR) $>$ 11.5 $L_{\odot}$, values between 2 and 7 for IRGs with $<$ 11.0 $<$ L(IR) $<$ 11.5 $L_{\odot}$, while lower values galaxies with L(IR) $<$ 11.0 $L_{\odot}$. The targeted lenses are characterised by large values of the $\frac{CO(7-6)}{CO(1-0)}$ ratio and have intrinsic IR luminosity, L(IR) $\geq 10^{13}L_{\odot}$. G12v2.43 has a $\frac{CO(7-6)}{CO(1-0)}$ value similar to the local starbursts and the Galactic centre, while the same ratio for the two other lenses is extreme and shows even more extreme conditions than ultra-luminous IR galaxies (ULIRGs). Note that the value shown in Figure 2 for NBv1.78 is actually $\frac{CO(7-6)}{CO(3-2)}$, still sensitive to total (warm, dense)/total H_2 gas mass, but the corresponding actual $\frac{CO(7-6)}{CO(1-0)}$ can be lower by a factor of up to ~ 3, depending of the global CO(3-2)/(1-0) line ratio (~0.3 for cold non-SF gas).

Low values of the CO ratios are typical of low infrared luminosity star-forming galaxies whose CO SLEDs are consistent with excitation by either photon-dissociation regions (PDRs) or mechanical excitation processes such as shocks and turbulence (Papadopoulos et al. 2012; Kamenetzky et al. 2017,and references therein). In more luminous galaxies, LIRGs and brighter, this ratio and the entire CO SLED, often cannot be explained solely by PDRs, because the ratio of the brightness of the high-J CO lines to lower-J lines would be too low without extreme densities, n $>10^{5}$cm^{-3}, and the far-infrared emission would be too faint given the CO line luminosities. Kamenetzky et al. (2016) report that the average SLEDs show increasing mid- to high-J CO luminosity relative to CO J = 1-0, from a few to ~100, with increasing L(IR). Even for the most luminous local galaxies, the high-J to J = 1-0 ratios do not exceed 180. In the Galaxy such CO line ratios can be that large only near compact hot regions in Galactic Molecular Clouds (GMCs), results of strong and localised excitation by intense far-UV radiation from OB stars (Papadopoulos et al. 2012).

In high luminosity galaxies, such as those of this work, different sources of excitation must be considered. One of these is the presence of the X-ray dominated regions (XDRs) where the chemistry is driven, instead of FUV photons, by X-ray photons that are able to penetrate deeper into the cloud without efficiently heating the dust at the same time. These X-rays are mostly produced by AGNs or in areas of extreme massive SF. CRs can also heat the gas by penetrating into cloud centers, similarly to X-rays, and are typically produced by supernovae (Bisbas et al. 2015). Mechanical heating is another efficient source of gas heating. This is commonly attributed to turbulence in ISM, which may be driven by supernovae, strong stellar winds, jets, galaxy mergers, cloud–cloud shocks, shear in the gaseous disk, or outflows (Meijerink et al. 2013; Rosenberg et al. 2015). These mechanisms, as main heating agents acting volumetrically on molecular gas clouds, unlike FUV photons, can create large mass fractions of $M_{WD}/M_{tot}(H_2)$. Such large masses of dense and warm gas are typical in merger-driven local starbursts (Papadopoulos et al. 2012), i.e. only in extreme environments where this gas fraction can reach roughly ten times the value found in quiescient galaxies (Papadopoulos et al. 2012, 2014; Lu et al. 2017).

Two of the three targets show also very large linewidths, so at least for G12v2.30 and NBv1.78 it can be interpreted as a possible sign of merger-driven velocity fields with expected large mechanical energy available as source of energy for their molecular gas. The presence of an AGN seems to be excluded as discussed in Omont et al. (2013) and Yang et al. (2016) from the measured 1.4 GHz radio fluxes. However, recently AGN signature has been found in one of the images of a lensed object, SDP9, (Massardi et al. 2017) and a hidden AGN contribution cannot be fully excluded. In the Local Universe, high-excitation galaxies with large linewidths are not necessarily associated with high AGN contributions and galaxies with large AGN contributions do not display necessarily large linewidths (Rosenberg et al. 2015), while low-excitation galaxies have smaller linewidths, and this narrowness is interpreted as the sign of radiative energy as major source of excitation.

Our three targets have gravitational lens magnifications μ of about 10 (Bussmann et al. 2013; Harris et al. 2012), determined from modeling the SMA continuum data at $880\mu m$. From these models alone, we cannot estimate how strong the differential lensing affects this result. If CO(7-6) and CO(1-0) emissions come from different and decoupled (not overlapping along the line of sight) regions the strong lensing effect may act differently on the two emissions, the resulting magnification would be different and the ratio would be altered. Yang et al. (2017) suggest that high-J CO lines may be magnified by a factor of at least 1.3 above the overall lensing magnification for CO(1-0), whose emission is expected to be more extended. The magnification factor by Yang et al. (2017) is derived by comparing the CO(1–0)/CO(3–2) ratio between a sample of unlensed SMG (Bothwell et al. 2013) and the H-ATLAS lensed SMGs. One would expect high-J CO could be more compact leaving this ratio rather a lower limit as stated above. Even if we allow the ratios shown in Figure 2 to decrease by this factor, the large detected excitation cannot be explained by differential lensing alone. It is worth noticing that if this were the case G12v.2.43 would fall within the boundaries of a photon-dominated ISM.

In Figure 3 we report the values of the $\frac{\mathrm{CO(7-6)}}{\mathrm{CI(2-1)}}$ of the lensed galaxies compared with values for the Local Universe (Kamenetzky et al. 2014; Rosenberg et al. 2015). Shown also in the Figure are the same ratios taken from the observations of similar objects by Walter et al. (2011); Yang et al. (2017). Papadopoulos & Geach (2012) suggested that the ratio between high-J CO line and the CI can be used as evidence for the SF mode, indicating whether a system is merger driven (large values) or disc-like (low values), where the difference can be up to a factor of 10 between these two types of systems. CI(2-1) is a good H_2 mass tracer (as long as $T_k \geq 30K$), even if CI(2-1) (or CI(1-0)) are yet to be well calibrated as H_2 global mass tracers (Joao et al. 2017).

For disc-dominated environments the $\frac{\mathrm{CO(7-6)}}{\mathrm{CI(2-1)}}$ ratio is expected to be lower than or roughly one, with the lowest value in the Outer Galaxy and quiescient clouds, while in merger-driven starbursts (ULIRGs and in the Galactic centre) this ratio may be a factor of ten larger. Papadopoulos & Geach (2012) suggest to use this ratio as well as a tracer of the ratio between the molecular mass in dense environments and the total molecular mass, $M_{WD}/M_{tot}(H_2)$ (Papadopoulos & Geach 2012,see also references therein). However, any differential lensing effects between the CI, which is easier to be excited, and the more extended emission with respect to the CO(7-6) emission would lower this ratio. If we were to consider the same factor as assumed for the CO(1-0) line, 1.3 less magnification than the higher-J CO lines for the CI(2-1), the corresponding ratio $\frac{\mathrm{CO(7-6)}}{\mathrm{CI(2-1)}}$ would be lower.

Even keeping in mind this effect, we can claim that most of the lensed high redshift objects lie in the range characteristic of large molecular gas excitation. Neutral atomic carbon remains abundant in H_2 gas over a large gas density range $100 \leq n \leq 10^4\ cm^{-3}$, i.e. the bulk of mass of typical molecular clouds. It only becomes markedly less abundant at higher densities where C becomes increasingly locked in CO (Glover et al. 2015), but also where much less H_2 gas mass resides in typical GMCs. However, for enhanced CR energy densities in these high redshift galaxies C can remain abundant even at higher gas densities (Bisbas et al. 2015).

3.2. Gas masses

We provide a rough estimate of H_2 mass using the expression in Papadopoulos (2005) (see also Weiss et al. 2005; Alaghband-Zadeh et al. 2013; Bothwell et al. 2017; Popping et al. 2017). However, a great source of uncertainty stems from the assumed excitation conditions that determine the gas excitation function, $Q(n,T)$, which without knowledge of the CI(1-0) luminosity cannot be estimated. Although the CI(1-0) is a better tracer of the molecular mass because of the smaller deviation of the $Q(n,T)$ value with respect to the local thermodynamical equilibrium (LTE) conditions ($\frac{Q_{1-0}}{Q_{1-0}^{(LTE)}} \sim 0.35 - 1$ $\frac{Q_{2-1}}{Q_{2-1}^{(LTE)}} \sim 0.15 - 1$, Papadopoulos et al. (2004)), we make here the following assumptions: (1) typical density of $100 < n < 5\ 10^4\ cm^{-3}$, (2) kinetic temperature, $T_k = 20 - 60K$, (3) T_k equivalent to the dust temperature. The latter has been estimated from the dust spectral energy distribution and the FIR luminosity (Zhang et al. 2018) and results are reported in Table 2 where also listed are the gas mass values computed for the three targets of this work.

The H_2 mass found assuming a (mass) carbon abundance (relative to the molecular hydrogen) of $X[CI] = M[CI] = 6M(H2) = 3\ 10^{-5}$ (Papadopoulos & Greve 2004; Papadopoulos et al. 2004; Weiss et al. 2005; Bothwell et al. 2017; Popping et al. 2017,and references therein) is compared to the molecular mass estimated from the CO line luminosity (Harris et al. 2012; Yang et al. 2017; Zhang et al. 2018).

Values in Table 3.2 are not corrected for magnification because we are not able to define it for CI. Our goal here is to compare the values found with the different tracers to show that CI can be used to estimate the molecular mass. With all the un-

Table 2. Magnification uncorrected values of the neutral Carbon and molecular masses

Galaxy	T_{dust} [a] (K)	M(CI) ($10^7 M_\odot$)	M(H_2) ($10^{11} M_\odot$)	M(H_2) [b] ($10^{11} M_\odot$)
G12v2.30	34	17±4	9.4±2.3	7.5±0.5
G12v2.43	31	<5.4	<3.0	1.3±0.8
NBv1.78	50	9.2±6.5	5.1±3.6	4.6 ± 0.5

Notes.
(a) data from Zhang et al. (2018); (b) data from CO(1-0) observations in Harris et al. (2012). A conversion factor between L(CO)′ and M(H_2) used is $0.8 M_\odot (\mathrm{K\ km\ s^{-1}\ pc^2})^{-1}$. For NBv1.78 estimated from CO(3-2) from Yang et al. (2017). Values are not corrected for magnification (see Table 1).

certainties listed above the agreement between the two estimations of the molecular masses is quite satisfactory.

3.3. Line - infrared luminosity ratios

In Figure 4 we show the distribution of the values of the luminosity ratio $CO(7-6)/FIR$ for the lensed and the local galaxies (Kamenetzky et al. 2016). The latter spans a wide range of values from 10^{-6} to 10^{-3}, with a median of 3.5 10^{-5}, but most of the galaxies - together with the ULIRGs - have values between 10^{-5} and 10^{-4}. Lowest value bins are occupied by galaxies as NGC1097, CenA, NGC891, while the largest value is that of a dwarf low-metallicity galaxy, NGC 4560.

If we very conservatively allow a factor of ten uncertainty because of the unknown effect of the gravitational lensing on the CO(7-6) emitting region and the overall FIR luminosity (which is likely due to the emission of the interstellar dust), the observed values for the three lenses show a wide range. The two lenses NBv1.78 and G12v2.30 have values largely exceeding the range defined by the local galaxies, consistent with that observed in NGC 6240 (Meijerink et al. 2013) and the Galaxy centre but still lower than those of NGC 4569. G12v2.43 has a value of $(0.1 - 1.3) \times 10^{-4}$ consistent with the values characteristics of the local IR galaxies. A result which confirms previous finding for SMGs and local galaxies (Lu et al. 2015). The large values $CO(7-6)/FIR$ (and also of $CI(2-1)/FIR$) in NBv1.78 and G12v2.30 are consistent with a chemistry driven by shocks (Pérez-Beaupuits et al. 2010). We note that shock, CR, or turbulent heating, quite unlike heating by FUV photons, do heat the dust as effectively as they do gas. Meijerink et al. (2013) find similar values in NGC6240, that they interpret as related to shocks, compressing the gas and heating it to higher temperatures, while not affecting the energy budget for the dust reservoir that remained comparatively much cooler. An even larger value is seen in NGC 4569 which is a low-IR luminosity galaxy in the Virgo cluster which shows evidence of ram pressure stripping, with a deficiency of atomic hydrogen but with a large presence of molecular gas (5 $10^9 M_\odot$) (Boselli et al. 2016).

The $CO(7-6)/FIR$ luminosity ratio shows a slight dependence on the IR luminosity as seen in other SMGs and lensed objects (Walter et al. 2011; Lu et al. 2015; Yang et al. 2017) but overall it is very cumbersome to quantify this dependence in cases where the presence of an AGN altering either the FIR or both luminosities cannot be excluded.

The $CO(7-6)$ luminosity is too large to be associated only to star formation rate processes as seen in local ULIRGs (Lu et al. 2015), but as discussed above without a detailed lensing model it is impossible to quantify the boosting of the different emitting components.

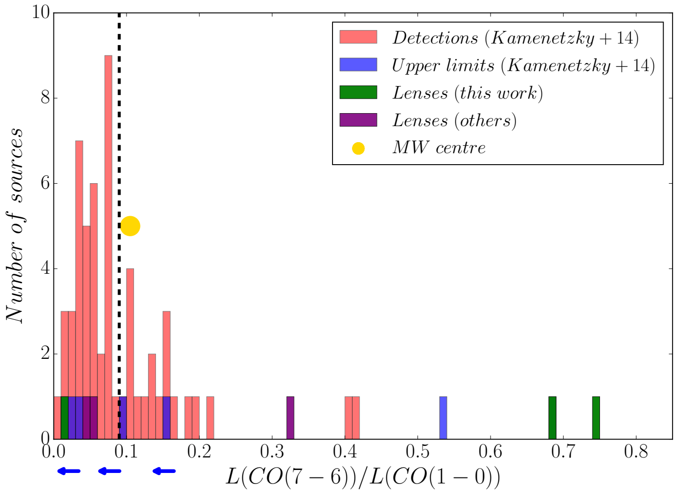

Fig. 2. Number of sources with a given CO(7-6)/CO(1-0) luminosity ratio (in units K km s^{-1} pc^2). Data from this work are marked in green, red (detections) and blue (upper limits) bars refer to detections and upper limits respectively taken from Kamenetzky et al. (2014). The value shown here for NBv1.78 is CO(7-6)/CO(3-2) (∼ 0.8) and the corresponding CO(7-6)/CO(1-0) is expected to be lower by a factor of ∼3. Data from other similar lensed targets are taken from Oteo et al. (2017); Yang et al. (2017) (shown in purple), Milky Way value from Fixsen et al. (1999) and corresponds to the centre of the Galaxy, values for the inner and outer Galaxy are upper limits (< 0.04 and < 0.07, respectively) and not shown here. Values between 0.15 and 0.4 correspond to LIRGs (L(IR) > 11.5$L_\odot$), values between 0.05 and 0.15 correspond to IRGs with (11.0 < L(IR) < 11.5$L_\odot$) and submillimetre galaxies, while lower values to galaxies with (L(IR) < 11.0$L_\odot$). Lenses detected in this work show values larger than those of the local ULIRGs. The black dashed vertical line marks the values below which the objects are FUV-photon dominated from those above which are non-FUV-photon heated (like NGC253, NGC6240, Arp220, the Galactic Centre, etc).

4. Conclusions

Three strongly lensed lensed galaxies at redshift $z \sim 3$ have been observed and detected with APEX/SEPIA5. The CO(7-6) emission has been detected in all three objects, while CI(2-1) in G12v2.30, marginally in NBv1.78 and not detected in G12v2.43.

The observed global $CO(7-6)/CI(2-1)$, $CO(7-6)/CO(1-0)$ and $CO(7-6)/L(FIR)$ luminosity ratios, when compared with well studied local galaxies, show evidence for some mechanism

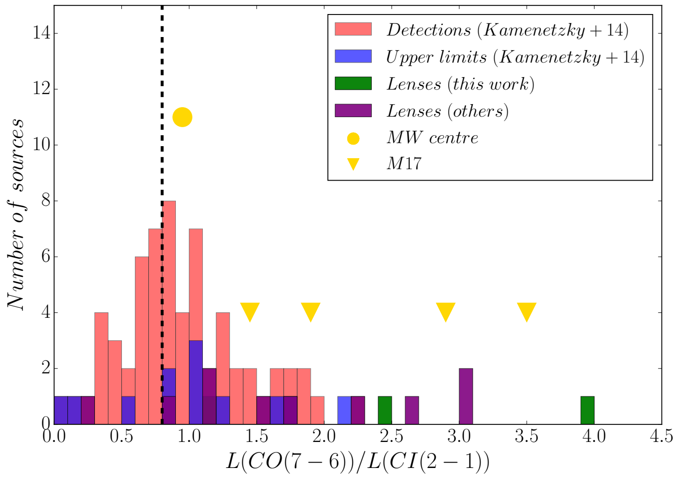

Fig. 3. Number of sources with a given CO(7-6)/CI(2-1) luminosity ratio (in units K km s^{-1} pc^2). Colour code as in Figure 2. Data for local galaxies are taken from Kamenetzky et al. (2014). A slight trend with IR luminosity is detected for the CO(7-6)/CI(2-1) ratio too, with larger values correspond to larger L(IR). For comparison with values found in star forming regions of the Galaxy, the range of ratios of M17 are also shown (Pérez-Beaupuits et al. 2010). Note that the blue bars correspond to upper limits (the objects have an upper limit on the CO(7-6) line emission), while for the two lenses G12v2.43 (~1.1) and NBv1.78 (~4) the green bars of correspond to lower limits and the corresponding ratio is larger. Added in this plot are the values of other lensed objects reported in Yang et al. (2017). The vertical dashed line indicates the value of the ratio $\frac{\mathrm{CO(7-6)}}{\mathrm{CI(2-1)}}$ below which the ISM is dominated by the FUV heating while those at larger values need other excitation mechanisms to explain the high value of the $\frac{\mathrm{CO(7-6)}}{\mathrm{CI(2-1)}}$.

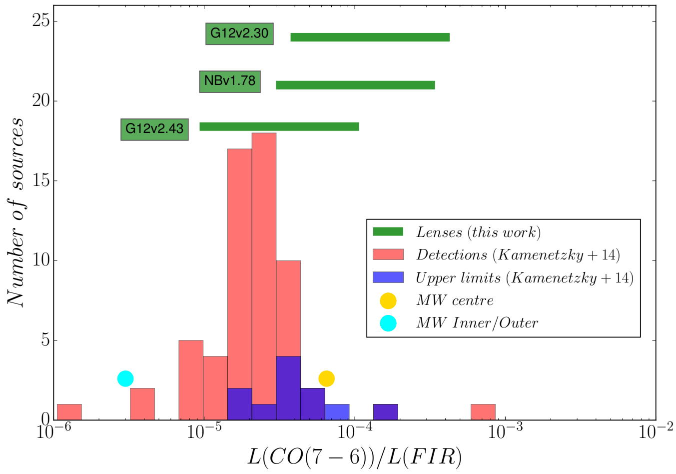

Fig. 4. Number of sources with a given CO(7-6)/FIR luminosity ratio. Colour code as in previous Figures.Data are taken from Kamenetzky et al. (2014). Values for the lens ratios show a range containing the observed values (Zhang et al. 2018) and an uncertainty of a factor of 10, likely comprehensive of the unknown effect of the gravitational lensing effect. For comparison the value of the Galaxy centre, inner and outer Galaxy are also shown hown (Fixsen et al. 1999).

other than the FUV-heating by star formation as the dominant power source for their molecular ISM. Mechanical energy in forms of shocks and/or strong turbulence and/or high CR energy densities can maintain large amounts of very warm and dense gas and then the average initial conditions of SF maybe no longer those found in less vigorously SF galaxies.

We have computed the molecular masses from the CI luminosity and find it in agreement with that derived from CO(1 − 0) within the uncertainties of both methods.

Higher angular resolution imaging together with a detailed lensing model is required to examine in detail the effect of the magnification on the different gas tracers, to discern the relative distributions of warm, dense gas associated with SF with respect to cooler, lower density gas (therefore altering their instrinsic ratios) and also probe the dynamics of these remarkable objects.

Acknowledgements. We would like to thank both the SEPIA team and the APEX operating team onsite for their hard work in making the SEPIA commissioning a success and for conducting PI observations. We would like to thank the referee for his/her suggestions to improve the readibility of the paper. APEX is a collaboration between the Max-Planck-Institut fur Radioastronomie, the European Southern Observatory (ESO), and the Onsala Space Observatory. SEPIA is a collaboration between Sweden and ESO.

References

Alaghband-Zadeh S., et al, 2013, MNRAS 435, 1493
Belitsky V. et al., 2017, A&A, in press, https://arxiv.org/abs/1712.07396
Billade B. et al., 2012, IEEE Trans. Terahertz Sci. Technol. 2, 208
Bisbas T.M. et al, 2015, ApJ 803, 37
Bisbas T.M. et al, 2017, ApJ 839, 90
Boselli A., et al., 2016, A&A 587, 68
Bothwell M.S. et al, 2013, MNRAS 429, 3047
Bothwell M.S. et al, 2017, MNRAS 466, 2825
Bradac M., et al., 2017, ApJ 836, L2
Bussmann R.S. et al, 2013, ApJ 779, 25;
Carilli C. & Walter F., 2013, ARAA 51, 10
De Breuck C. et al, 2014, A&A 565, 59
Fixsen D.J., Bennett C. L., and Mather J. C., 1999, ApJ 526, 207
Fu H., et al, 2012, ApJ 753, 134
Gerin M. & Phillips T., 2000, ApJ 537, 644
Glover S.C. & Clark P.C., 2016, MNRAS 456, 3596
Glover S.C. et al., 2015, MNRAS 448, 1607
Güsten R., Nyman L. Å., Schilke P., Menten K., Cesarsky C., Booth R., 2006, A&A 454, 13
Joao et al., 2017, ApJ 840, L18
Harris A.I. et al, 2012, ApJ 752, 152
Hayatsu N. H. et al., 2017, PASP 69, 45
Kamenetzky J., Rangwala N., Glenn J., Maloney P. R., Conley A., 2014, ApJ 795, 174
Kamenetzky J., Rangwala N., Glenn J., Maloney P. R., Conley A., 2016, ApJ 829, 93
Kamenetzky J., Rangwala N., Glenn J., 2017, MNRAS 471, 2917
Knudsen K. et al, 2016, MNRAS 462, L6
Immer K., et al., 2016, The Messenger 165, 13
Lu N. et al., 2015, ApJ 802, L11
Lu N. et al., 2017, ApJ Supp 230, 1L
Massardi M., et al., 2017 arXiv170910427M
Meijerink R., Kristensen L. E, Weiß A., van der Werf P. P., Walter F., Spaans M., Loenen A. F., et al., 2013, ApJ 762, L16
Omont A. et al, 2013, A&A 551, 115
Oteo I., et al., 2017, https://arxiv.org/abs/1701.05901
Papadopoulos P.P. and Greve T., 2004, ApJ 615, L29
Papadopoulos P.P., Thi W.F., Viti S., 2004, MNRAS 351, 147
Papadopoulos P.P., 2005, ApJ 623, 763
Papadopoulos P.P., et al, 2010, ApJ 715, 775
Papadopoulos P.P., et al, 2012, MNRAS 426, 2601
Papadopoulos P.P. & Geach J.E., 2012, ApJ 757, 157
Papadopoulos P.P., et al, 2014, ApJ 788, 153
Pérez-Beaupuits J. P., Spaans M., Hogerheijde M.R., Günten R., Baryshev A., Boland W., 2010, A&A 510, A87
Pety J., et al, 2004, A&A 428, 21
Popping G., et al, 2017, A&A 602, 11
Rosenberg M.J.F., et al., 2015, ApJ 801, 72
Saito T., et al., 2017, ApJ 835, 174
Solomon P.M. et al., 1997, ApJ 478, 144
Tomassetti M., Porciani E., Romano-Díaz E., Ludlow A.D., Papadopoulos P.P., 2014, MNRAS 445, L124
Yang C. et al, 2016, A&A 595, A80
Yang C. et al., 2017, arXiv170904740Y
Walter F., et al., 2115, ApJ 730, 18
Weiss A., et al., 2005, A&A 429, L25
Zhang, Z.-Y., et al., 2014 A&A 568, A122
Zhang, Z.-Y., Papadopoulos, P. P., Ivison, R. J., et al. 2016, Royal Society Open Science, 3, 160025
Zhang, Z.-Y. et al., 2018, in preparation